A&A 635, A65 (2020)
https://doi.org/10.1051/0004-6361/201936843

Astronomy & Astrophysics

The binary content of multiple populations in NGC 3201

S. Kamann[1], B. Giesers[2], N. Bastian[1], J. Brinchmann[3,4], S. Dreizler[2], F. Göttgens[2], T.-O. Husser[2], M. Latour[2], P. M. Weilbacher[5], and L. Wisotzki[5]

[1] Astrophysics Research Institute, Liverpool John Moores University, 146 Brownlow Hill, Liverpool L3 5RF, UK
e-mail: s.kamann@ljmu.ac.uk
[2] Institute for Astrophysics, Georg-August-Universität Göttingen, Friedrich-Hund-Platz 1, 37077 Göttingen, Germany
[3] Instituto de Astrofísica e Ciências do Espaço, Universidade do Porto, CAUP, Rua das Estrelas, 4150-762 Porto, Portugal
[4] Leiden Observatory, Leiden University, PO Box 9513, 2300 RA Leiden, The Netherlands
[5] Leibniz-Institute for Astrophysics, An der Sternwarte 16, 14482 Potsdam, Germany

Received 4 October 2019 / Accepted 5 February 2020

ABSTRACT

We investigate the binary content of the two stellar populations that coexist in the globular cluster NGC 3201. Previous studies of binary stars in globular clusters have reported higher binary fractions in their first populations (P1, having field-like abundances) compared to their second populations (P2, having anomalous abundances). This is interpreted as evidence for the latter forming more centrally concentrated. In contrast to previous studies, our analysis focusses on the cluster centre, where comparable binary fractions between the populations are predicted because of short relaxation times. However, we find that even in the centre of NGC 3201, the observed binary fraction of P1 is higher (23.1 ± 6.2)% compared to (8.2 ± 3.5)% in P2. Our results are difficult to reconcile with a scenario in which the populations only differ in their initial concentrations, but instead suggests that the populations also formed with different fractions of binary stars.

Key words. binaries: spectroscopic – techniques: radial velocities – globular clusters: individual: NGC 3201 – stars: abundances

1. Introduction

One of the lesser studied aspects of the multiple populations (also known as abundance anomalies, see Bastian & Lardo 2018, for a review) phenomena in massive stellar clusters is the role of stellar binarity. This is due to the overall relatively low binary fractions in globular clusters (GCs; e.g. Ji & Bregman 2015) and the fact that it is difficult to separate out the binaries from (apparent) single stars in colour-magnitude diagrams for each of the populations (i.e. the "normal" and "anomalous" stars; P1 and P2) as the sequences overlap. Instead, we must carry out intensive spectroscopic time-series analyses of a representative sample of stars from each population to search for radial velocity variations.

The most comprehensive survey using this technique, to date, is that of Lucatello et al. (2015) who monitored 968 red giant branch (RGB) stars in ten Milky Way ancient GCs. From this large sample these authors find 21 binary stars and when separating their sample into P1 and P2 stars, find binary fractions of 4.9% and 1.2% for each population, respectively. In addition, Dalessandro et al. (2018) report a higher binary fraction in P1 of the GC NGC 6362, 14% compared to <1% in P2.

Such differences can be explained in terms of the formation environment of the stars; the P2 stars (lower binary fraction) form and initially evolve in a much denser environment, which would destroy many of the primordial binaries (e.g. Hong et al. 2016). An initially more concentrated P2 is a common feature of essentially all scenarios put forward to explain multiple populations and appears to be in agreement with the observed density profiles and kinematics of the populations in most Galactic GCs today (e.g. Lardo et al. 2011; Richer et al. 2013; Bellini et al. 2015; Dalessandro et al. 2019).

As a consequence of the fibre-based observations, the targets for the study of Lucatello et al. (2015) are preferentially located in the outer regions of the clusters. Most GCs show a trend of increasing binary fractions towards the cluster centres (e.g. Milone et al. 2012), which is thought to be due to mass segregation. On the other hand, dynamical processes lowering the binary fractions, such as binary disruption or ejection from the cluster, occur more frequently near to the cluster centres. Therefore, the binary statistics near to the cluster centres may not follow those in the cluster outskirts. Using *N*-body simulations, Hong et al. (2015, 2016) find that the binary fractions of P2 are expected to be comparable or even larger than those of P1 inside the half-light radii of the clusters if P2 formed centrally concentrated.

In the present work we explicitly test these predictions, using the time series VLT/MUSE observations of NGC 3201, stretching over more than four years, presented in Giesers et al. (2019), which focus on the region inside the core radius (r_c = 1.3′ ≡ 1.85; Harris 1996) of the cluster. RGB stars from the different populations are found using a UV-optical "chromosome map" (Milone et al. 2017), which is highly efficient in separating the populations, largely based on their *N* abundance differences (Lardo et al. 2018).

2. Data

NGC 3201 has been observed as part of the MUSE survey of Galactic GCs (see Kamann et al. 2018), a large GTO programme targeting the central regions of massive star clusters. To facilitate the detection and characterisation of binary stars, repeated observations of five pointings, covering approximately the central 2′×2′ of the cluster, were performed from November 2014 to

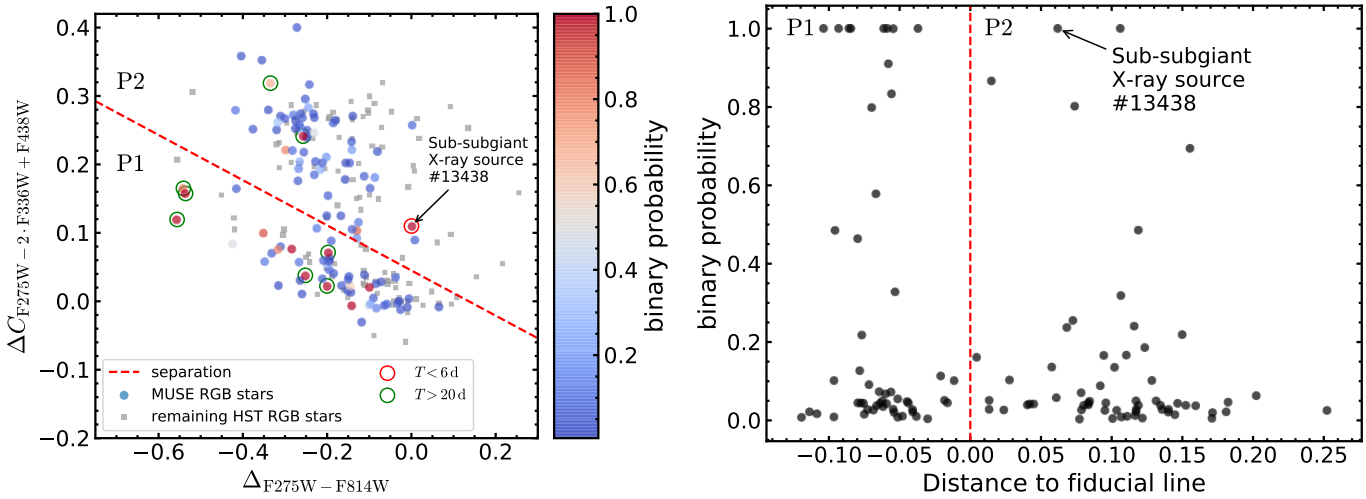

Fig. 1. *Left*: distribution of red giant stars in NGC 3201 in pseudo-colour space, the so-called chromosome map. The full sample of stars obtained from the HST photometry of Piotto et al. (2015) is shown as small grey dots. Stars available in the MUSE sample are highlighted and colour-coded according to their probability of being in a binary system. For the sub-sample of MUSE sources with known Keplerian parameters, coloured rings indicate the orbital period T. The dashed red line illustrates our separation into P1 and P2 stars. *Right*: the binary probability of the stars in the MUSE sample is shown as a function of the distance of a star perpendicular to the line separating P1 and P2 (i.e. the dashed red line in the *left panel*).

May 2019. The data analysis, including the detection and characterisation of binaries, are described in Giesers et al. (2019). For each of the 3 553 stars studied, the authors provided a probability that the star shows radial velocity variations. The radial velocities of the stars with at least five observations and with a probability higher than 50% of being variable were further analysed with THE JOKER (Price-Whelan et al. 2018), resulting in a subset of 95 stars with unique Keplerian orbit solutions.

To split up the two stellar populations that have previously been identified in NGC 3201, we used the *Hubble* Space Telescope (HST) photometry from the survey of Piotto et al. (2015, see Nardiello et al. 2018). As outlined in Latour et al. (2019), this was done by creating a "chromosome map" from the red giant stars (see Milone et al. 2015), which is shown in Fig. 1. The separation of the two populations was performed following Milone et al. (2017) and is indicated by the red dashed line included in Fig. 1 (with P1 being below the fiducial line).

Finally, we identified the subset of stars from Giesers et al. (2019) for which the population could be determined. This resulted in a final sample of 113 stars, 52 in P1, and 61 in P2, which is presented in Table A.1. For the 17 out of 113 stars which had a probability $P > 0.5$ of being in a binary and sufficient ($\geq$5) observations, we tried to determine the Keplerian orbit. This resulted in a subset of nine stars, for which an orbit solution is available. The orbital parameters of said stars are included in Table A.1. The remaining eight stars with $P > 0.5$ have insufficient kinematical data to infer their Keplerian orbits.

3. Results

3.1. Binaries across the chromosome map

The distribution of binary stars across the chromosome map of NGC 3201 is shown in the left panel of Fig. 1. We colour-coded each star available in the sample of Giesers et al. (2019) by its probability to be in a binary system. Stars for which orbital solutions have been found are further highlighted according to their orbital period T. To better visualise possible differences between P1 and P2, we show the binary probability as a function of the distance perpendicular to the fiducial line separating P1 and P2 in the right panel of Fig. 1.

To infer the binary fractions in both populations, we followed Giesers et al. (2019) and obtain the fraction of stars with a binary probability of $P > 0.5$ within each population. This leads to binary fractions of $(23.1 \pm 6.2)\%$ in P1 and $(8.2 \pm 3.5)\%$ in P2. The uncertainties tailored to both values take into account the limited sample sizes as well as the uncertainties stemming from the threshold in P (see Giesers et al. 2019, for details). When calculating the binary fraction in P2, we included the sub-subgiant star highlighted in Fig. 1, which is in a much tighter orbit than the remaining binary systems (indicated by the coloured rings in Fig. 1). As discussed in Giesers et al. (2019), this star has an X-ray counterpart and shows Hα emission. Hence it is plausible that this star is part of an accreting binary system, which would also impact its photometric properties and its location in the chromosome map. Excluding it from our calculation reduces the binary fraction of P2 to $(6.7 \pm 3.3)\%$. Averaged over both populations, we find a binary fraction of $(15.0 \pm 3.4)\%$, in good agreement with the discovery fraction of $(17.1 \pm 1.9)\%$ determined by Giesers et al. (2019).

3.2. Origin of the observed binaries

To study the origin of the observed binaries, we made use of the subsample with known orbital parameters. The fate of a binary in a GC is linked to its hardness h, that is the ratio of its internal energy $\tilde{E}$ to the average kinetic energy of the surrounding stars,

$$h = |\tilde{E}|/m\sigma^2, \quad (1)$$

where m is the typical stellar mass of a cluster member and σ the velocity dispersion of the cluster. For a bound Keplerian orbit, the internal energy is given as

$$\tilde{E} = -\frac{Gm_\mathrm{p}m_\mathrm{c}}{2a}, \quad (2)$$

where m_p and m_c are the masses of the constituents and a is the semi-major axis of the binary. In Table A.1, we provide the

hardness for each binary with an orbit available. The values were calculated assuming an inclination of $i = 90°$ (i.e. the minimum possible companion mass m_c). The mass of the primary (RGB) component, m_p, was determined via comparison to an isochrone as described in Giesers et al. (2019). As cluster properties, we used $m = 0.8\,M_\odot$ and $\sigma = 4.3\,\mathrm{km\,s^{-1}}$ (Baumgardt & Hilker 2018). All systems are hard binaries with $h > 1$, indicating that they can survive in NGC 3201 for a Hubble time. Their longevity can be confirmed by determining the expected lifetimes of the binary stars, $\tau = 1/B(\tilde{E})$, where $B(\tilde{E})$ is the probability of a binary being ionised (i.e. destroyed) in a gravitational encounter with a third cluster member, given as (Eq. (7.174) in Binney & Tremaine 2008)

$$B(\tilde{E}) = \frac{8\sqrt{\pi}G^2m^3\rho\sigma}{3^{3/2}|\tilde{E}|}\left(1+\frac{1}{5h}\right)^{-1}\left[1+e^h\right]^{-1}. \quad (3)$$

Evaluating Eq. (3) for a core density of $\rho = 10^{2.72}\,M_\odot/\mathrm{pc}^3$ (Baumgardt & Hilker 2018) yields lifetimes for all binary stars that exceed the age of NGC 3201 by several orders of magnitude.

We note that the companion masses m_2 and the semi-major axes a used in the above calculations were derived under the assumption that the binaries are observed edge-on (i.e. at an inclination of $i = 90\,\mathrm{deg}$). While both quantities increase with decreasing inclinations, m_2 is more sensitive on i than a is, so that our hardness values can be considered as lower limits.

Finally, we stress that the probability to form hard binaries dynamically in a relatively low-density cluster such as NGC 3201 is very small. Using Eq. 7.176 from Binney & Tremaine (2008), the formation rate of hard binaries per unit volume is given as

$$C_{\mathrm{hb}} = 0.74\frac{G^5\rho^3m^2}{\sigma^9}. \quad (4)$$

Integrating Eq. (4) over the core of NGC 3201 (assuming $r_c = 1.74$; Baumgardt & Hilker 2018) yields a total formation rate of $7\times10^{-6}\,\mathrm{Gyr}^{-1}$. Hence it is very likely that all binary stars that we observe in NGC 3201 are primordial.

3.3. Impact of the companion

Our determination of the binary fraction in each population is based on the assumption that the positions of the stars in the chromosome map are not altered by the presence of their companions. To verify this assumption, we used the binaries with known orbits and inferred the magnitude changes caused by their companions in the four HST filters underlying the chromosome map, $F275W$, $F336W$, $F438W$, and $F814W$. To this aim, we fetched an isochrone tailored to the properties of NGC 3201 ([Fe/H] = −1.59, $E_{B-V} = 0.24$; Harris 1996) from the MIST database (Choi et al. 2016). We made the assumption that the companions are main-sequence stars and predicted their magnitudes $\mathrm{mag_c}$ by selecting the isochrone points along the main sequence closest to their measured masses, $m_c \sin i$ (cf. Table A.1). As the measured companion masses need to be corrected for the (unknown) orbit inclinations relative to the line of sight, we assumed different inclination angles i and found the isochrone counterpart for each value of m_c. At each inclination, we calculated the corrected magnitude $\mathrm{mag_p}$ of the RGB star in the four relevant filters, according to

$$\mathrm{mag_p} = \mathrm{mag_{tot}} - 2.5\log_{10}\left(1-10^{-0.4(\mathrm{mag_c}-\mathrm{mag_{tot}})}\right), \quad (5)$$

where $\mathrm{mag_{tot}}$ is the measured magnitude of the system in the considered filter. Then we predicted the actual location of each RGB star in the chromosome map. We stopped when subtracting the contribution of a fiducial companion resulted in a predicted position that was off by more than 0.1 mag from the red edge of the RGB in either $(F275W - F814W)$ colour or $(F275W - 2\cdot F336W + F438W)$ pseudo-colour.

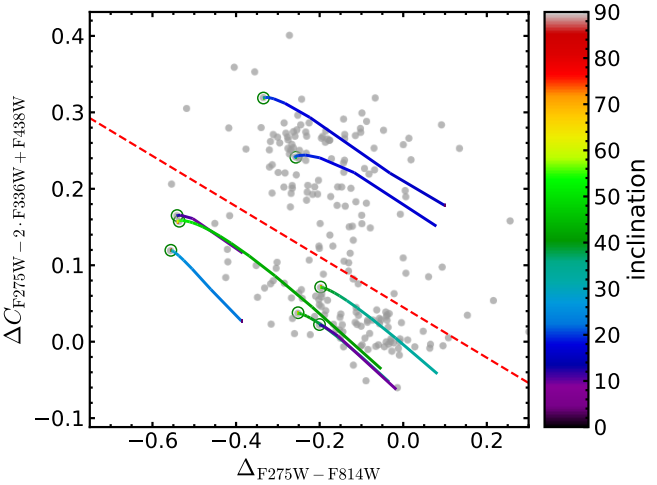

Fig. 2. Impact of binary companions on the positions of RGB stars in the chromosome map of NCG 3201. For each star from our sample with known orbit, the true position of the RGB star after subtracting the contribution of a main-sequence companion, as a function of orbit inclination, is shown. The grey points and dashed red line are the same as in the left panel of Fig. 1.

We summarise the outcome of this test in Fig. 2. It shows the predicted position of the RGB star in the chromosome map as a function of the inclination for each binary in our sample with a known orbit. Figure 2 shows that P2 stars in a binary with a main-sequence star are very unlikely to appear as P1 stars (and vice versa), as the companion tends to shift the binary in a direction parallel to the fiducial line separating the populations.

We further find that the companion needs to be massive enough to appear close to the main-sequence turn-off to have a significant effect. Figure 2 shows that for all of the sources in our sample, their orbits would need to be observed at low inclinations, $i \lesssim 40°$, in that case, because our minimum masses are significantly below the expected turn-off mass of NGC 3201 ($m_{\mathrm{TO}} \sim 0.8\,M_\odot$; cf. Table A.1). Under the assumption of randomly orientated orbits, we can estimate the probabilities to observe the systems at or below the inclinations where the companions have a measurable effect on the observed positions in the chromosome map. We find probabilities between <1% and about 35% for the individual systems. Considering the sum of probabilities for the eight stars, we expect about one star among the eight to have been measurably shifted by its companion. We note that these probabilities do not account for the selection bias of radial velocity studies, which are more sensitive to edge-on orbits, and hence can be considered as upper limits (see discussion in Carroll & Ostlie 2006).

We also considered the possibility of white-dwarf companions, as they may have a stronger impact on the $F275W$ flux. However, in the photometry of Nardiello et al. (2018), we find only 10–15 white dwarf candidates with a $F275W$ magnitude within 2 mag of the main-sequence turn-off.

4. Discussion

At first glance, our finding of a lower binary fraction in P2 than in P1 agrees with previous studies on the binary content

of multiple populations (Lucatello et al. 2015; Dalessandro et al. 2018). This trend was attributed to the P2 stars forming centrally concentrated, resulting in a higher rate of binary ionisation and ejection. However, in contrast to earlier studies, our observations focus on the dense cluster core. In the simulations of Hong et al. (2015, 2016), the overabundance in P1 binaries typically only develops outside the half-light radii of the simulated clusters, whereas the trend disappears or even reverses inside of this radius[1]. The observation by Dalessandro et al. (2018) that the discrepancy in the observed velocity dispersions between P1 and P2 stars in NGC 6362, which is attributed to the overabundance of P1 binaries, disappears towards the centre can also be interpreted as a hint about comparable central binary fractions.

Compared to the clusters simulated by Hong et al. (2015, 2016), where all stars were input with the same masses, NGC 3201 appears much more complex. One complication is the likely presence of a large population of stellar-mass black holes (Giesers et al. 2018, 2019; Askar et al. 2018), which is expected to have a strong impact on the evolution of NGC 3201. Owing to their masses, black holes can efficiently suppress the segregation of the binaries to the cluster centre. As the evolution of a binary population is governed by the interplay between mass segregation and their interactions with other stars, this marks an important difference compared to the existing simulations. Dedicated simulations using a realistic range of stellar masses will be an important step forward towards understanding the evolution of binary stars in multiple populations.

A possible explanation for our results is that P2 had different binary properties than P1 upon formation, for example a lower primordial binary fraction or a different distribution of semi-major axes. Most formation scenarios predict P2 stars to form while at least part of the P1 population is already in place. It seems likely that such vastly different formation environments had an impact on the properties of the primordial binaries in P2. Future hydrodynamical simulations of cluster formation may be able to investigate this further.

We note that some of the detected P1 binaries appear in a region of the chromosome map that is termed the extended P1 (e.g. Lardo et al. 2018), that is to the top left of the bulk of P1 stars. As shown by for example Cabrera-Ziri et al. (2019), extended P1 stars show no differences in their abundances of C, N, O, Na, Mg, or Al compared to normal P1 stars. Marino et al. (2019) argue that binaries could be responsible for creating extended P1 stars in NGC 3201 (also see Martins et al. 2020). As our analysis of Sect. 3.3 shows, normal P1 stars in binary systems with main-sequence stars close to the turn-off can be shifted into the extended branch. However, it appears unlikely that this scenario is responsible for all of the stars observed along the extended P1. The binary systems with unique orbital solutions would need to be observed at rather unlikely inclination angles for the companions to produce noticeable shifts. In addition, a number of extended P1 stars do not show any signs of variability in our sample. Nevertheless, extending our analysis to other clusters with a pronounced extended P1, such as NGC 2808, appears to be a very promising step in studying the impact of binary stars on the distribution of stars across chromosome maps.

Finally, we note that in comparison to Marino et al. (2019), our extended P1 extends to smaller values of $\Delta_{F275W-F814W}$. Upon removal of the stars with $\Delta_{F275W-F814W} \lesssim -0.4$, which were not considered in the work by Marino et al. (2019), our P1 binary fraction reduces to $19.1 \pm 5.7\%$. Hence our main conclusion of a higher binary fraction in P1 than in P2 does not depend on the exact definition of which stars belong to P1.

Acknowledgements. SK and NB gratefully acknowledge funding from a European Research Council consolidator grant (ERC-CoG-646928- Multi-Pop). BG, SD, TOH, and ML acknowledge funding from the Deutsche Forschungsgemeinschaft (grant DR 281/35-1 and KA 4537/2-1) and from the German Ministry for Education and Science (BMBF Verbundforschung) through grants 05A14MGA, 05A17MGA, 05A14BAC, and 05A17BAA. NB gratefully acknowledges financial support from the Royal Society in the form of a University Research Fellowship. JB acknowledges support by FCT/MCTES through national funds (PIDDAC) by grant UID/FIS/04434/2019 and through Investigador FCT Contract No. IF/01654/2014/CP1215/CT0003.

References

Anderson, J., Sarajedini, A., Bedin, L. R., et al. 2008, AJ, 135, 2055
Askar, A., Arca Sedda, M., & Giersz, M. 2018, MNRAS, 478, 1844
Bastian, N., & Lardo, C. 2018, ARA&A, 56, 83
Baumgardt, H., & Hilker, M. 2018, MNRAS, 478, 1520
Bellini, A., Vesperini, E., Piotto, G., et al. 2015, ApJ, 810, L13
Binney, J., & Tremaine, S. 2008, Galactic Dynamics: Second Edition (Princeton: Princeton University Press)
Cabrera-Ziri, I., Lardo, C., & Mucciarelli, A. 2019, MNRAS, 485, 4128
Carroll, B. W., & Ostlie, D. A. 2006, An Introduction to Modern Astrophysics and Cosmology (San Francisco: Addison-Wesley)
Choi, J., Dotter, A., Conroy, C., et al. 2016, ApJ, 823, 102
Dalessandro, E., Mucciarelli, A., Bellazzini, M., et al. 2018, ApJ, 864, 33
Dalessandro, E., Cadelano, M., Vesperini, E., et al. 2019, ApJ, 884, L24
Giesers, B., Dreizler, S., Husser, T.-O., et al. 2018, MNRAS, 475, L15
Giesers, B., Kamann, S., Dreizler, S., et al. 2019, A&A, 632, A3
Harris, W. E. 1996, AJ, 112, 1487
Hong, J., Vesperini, E., Sollima, A., et al. 2015, MNRAS, 449, 629
Hong, J., Vesperini, E., Sollima, A., et al. 2016, MNRAS, 457, 4507
Ji, J., & Bregman, J. N. 2015, ApJ, 807, 32
Kamann, S., Husser, T.-O., Dreizler, S., et al. 2018, MNRAS, 473, 5591
Lardo, C., Bellazzini, M., Pancino, E., et al. 2011, A&A, 525, A114
Lardo, C., Salaris, M., Bastian, N., et al. 2018, A&A, 616, A168
Latour, M., Husser, T. O., Giesers, B., et al. 2019, A&A, 631, A14
Lucatello, S., Sollima, A., Gratton, R., et al. 2015, A&A, 584, A52
Marino, A. F., Milone, A. P., Sills, A., et al. 2019, ApJ, 887, 91
Martins, F., Morin, J., Charbonnel, C., Lardo, C., & Chantereau, W. 2020, A&A, 635, A52
Milone, A. P., Piotto, G., Bedin, L. R., et al. 2012, A&A, 540, A16
Milone, A. P., Marino, A. F., Piotto, G., et al. 2015, MNRAS, 447, 927
Milone, A. P., Piotto, G., Renzini, A., et al. 2017, MNRAS, 464, 3636
Nardiello, D., Libralato, M., Piotto, G., et al. 2018, MNRAS, 481, 3382
Piotto, G., Milone, A. P., Bedin, L. R., et al. 2015, AJ, 149, 91
Price-Whelan, A. M., Hogg, D. W., Rix, H.-W., et al. 2018, AJ, 156, 18
Richer, H. B., Heyl, J., Anderson, J., et al. 2013, ApJ, 771, L15

[1] In contrast to Hong et al. (2015, 2016), we can only infer the binary fractions as a function of projected radius.

Appendix A: Table

Table A.1. Photometric and orbital properties of the binaries with unique *Kepler* solutions in the MUSE sample.

ACS Id	$\Delta_{275,814}$	$\Delta C_{275,336,438}$	Pop.	$P_{\rm bin}$	$m_{\rm p}/M_\odot$	$m_{\rm c}\sin i/M_\odot$	a/AU [(a)]	e	T/d	h
3092	0.064	−0.008	1	0.006						
3248	0.000	0.257	2	0.065						
3795	−0.142	0.222	2	0.188						
4121	−0.424	0.084	1	0.486						
4125	−0.320	0.251	2	0.027						
4566	−0.225	0.107	1	0.103						
4698	−0.243	0.317	2	0.049						
4853	−0.119	−0.030	1	0.019						
5281	−0.348	0.059	1	0.103						
5461	−0.201	0.125	2	0.030						
6228	−0.195	0.063	1	0.047						
6560	−0.127	0.116	2	0.105						
10705	−0.311	0.271	2	0.024						
10741	−0.265	0.031	1	0.011						
10753	−0.065	−0.005	1	0.028						
10968	−0.262	0.253	2	0.242						
11180	0.007	0.090	2	0.044						
11203	−0.265	0.204	2	0.239						
11273	−0.168	0.125	2	0.029						
11281	−0.130	0.104	2	0.866						
11294	−0.196	0.047	1	0.070						
11305	−0.085	0.026	1	0.050						
11306	−0.082	0.219	2	0.023						
11317	−0.252	0.038	1	1.000	0.83	0.42	1.5	0.249	603	6.64
11425	−0.147	0.202	2	0.028						
11455	−0.351	0.100	1	0.910						
11585	−0.201	0.056	1	0.329						
11750	−0.231	0.185	2	0.060						
11806	−0.088	0.181	2	0.137						
11821	−0.316	0.024	1	0.010						
11888	−0.245	0.283	2	0.221						
11918	−0.166	0.024	1	0.030						
11942	−0.141	0.106	2	0.053						
12115	−0.339	0.280	2	0.015						
12253	−0.268	0.194	2	0.138						
12309	−0.217	0.193	2	0.257						
12319	−0.267	0.058	1	0.093						
12322	−0.228	0.205	2	0.040						
12363	−0.112	0.039	1	0.024						
12468	−0.260	0.011	1	0.024						
12517	−0.186	0.261	2	0.046						
12646	−0.415	0.165	1	0.047						
12658	−0.198	0.071	1	1.000	0.83	0.40	0.659	0.073	176	14.7
12833	−0.263	0.274	2	0.030						
13019	−0.191	0.089	1	0.053						
13112	−0.299	0.221	2	0.802						
13174	−0.153	0.016	1	0.046						
13438	0.000	0.110	2	1.000	0.82	0.35	0.0676	0.022	5.93	123
13521	−0.195	0.059	1	0.013						
13556	−0.310	0.080	1	0.045						
13739	−0.417	0.279	2	0.090						
13768	−0.073	0.029	1	0.012						
13808	−0.334	0.319	2	0.695	0.83	0.21	4.13	0.112	3e+03	1.24
13816	−0.541	0.165	1	0.834	0.83	0.11	0.864	0.166	302	3.19
13824	−0.247	0.243	2	0.168						
14175	−0.209	0.060	1	0.057						
14302	−0.091	0.006	1	0.040						
14465	−0.259	0.268	2	0.052						

Notes. For each star, we provide the ID in the photometric catalogue of Anderson et al. (2008), the location in the chromosome map, the population tag, the binary probability, the mass of the primary star, the minimum mass of the companion star, the semi-major axis, eccentricity, and period of the orbit, and its hardness. [(a)]Assuming the orbit is orientated edge-on (i.e. $i = 90$ deg).

Table A.1. continued.

ACS Id	$\Delta_{275,814}$	$\Delta C_{275,336,438}$	Pop.	$P_{\rm bin}$	$m_{\rm p}/M_{\odot}$	$m_{\rm c}\sin i/M_{\odot}$	a/AU [(a)]	e	T/d	h
14601	−0.331	0.071	1	0.047						
14789	−0.059	−0.003	1	0.075						
14815	−0.248	0.250	2	0.030						
14830	−0.404	0.358	2	0.022						
15012	−0.035	−0.002	1	0.074						
15013	−0.280	0.272	2	0.104						
15069	−0.233	0.274	2	0.016						
15101	−0.212	0.203	2	0.047						
15165	−0.157	0.202	2	0.007						
15182	−0.144	0.014	1	0.018						
15293	−0.536	0.158	1	1.000	0.82	0.49	1.64	0.477	669	7.16
15382	−0.146	0.023	1	0.579						
15422	−0.143	0.234	2	0.041						
15482	−0.284	0.077	1	1.000						
15528	−0.300	0.267	2	0.052						
20774	−0.270	0.176	2	0.042						
21050	−0.202	0.211	2	0.167						
21060	−0.084	−0.009	1	0.129						
21131	−0.039	0.036	1	0.115						
21189	−0.158	0.178	2	0.005						
21232	−0.142	−0.006	1	1.000						
21271	−0.027	−0.012	1	0.051						
21272	−0.252	0.296	2	0.039						
21273	−0.282	0.221	2	0.072						
21292	−0.113	0.183	2	0.047						
21707	−0.249	0.240	2	0.011						
21918	−0.275	0.264	2	0.008						
21921	−0.101	0.021	1	0.999						
22325	−0.099	0.166	2	0.042						
22396	−0.011	−0.008	1	0.022						
22401	−0.130	0.093	2	0.163						
22488	−0.317	0.262	2	0.320						
22686	−0.376	0.252	2	0.029						
22751	−0.556	0.120	1	1.000	0.83	0.30	0.631	0.027	173	11.4
23045	−0.255	0.218	2	0.051						
23175	−0.200	0.022	1	1.000	0.83	0.12	0.491	0.124	129	5.78
23330	−0.030	0.001	1	0.010						
23342	−0.101	−0.005	1	0.465						
23375	−0.232	0.246	2	0.487						
23452	−0.257	0.241	2	1.000	0.82	0.20	0.69	0.056	206	7.01
23461	−0.181	0.265	2	0.040						
23519	−0.212	0.034	1	0.046						
23640	−0.198	0.155	2	0.044						
24190	−0.140	0.271	2	0.007						
24416	−0.276	0.253	2	0.012						
24524	−0.098	−0.003	1	0.220						
24592	−0.151	0.033	1	0.045						
24594	−0.355	0.352	2	0.024						
24684	−0.272	0.400	2	0.028						
24753	−0.007	0.005	1	0.030						
24803	−0.149	0.037	1	0.031						
24832	−0.266	0.258	2	0.040						
24875	−0.231	0.269	2	0.030						
25058	−0.185	0.041	1	0.037						
25322	−0.317	0.076	1	0.799						